

## Performance Analysis of a Modified Three-Phase Induction Motor with Optimal Capacitance fed by Single-Phase AC Supply

**Abstract.** This paper proposes a performance analysis of a modified three-phase induction motor with optimal capacitance operating with a single-phase mains supply. The modified three-phase motor is described and analyzed. Based on analytical equations, calculation of optimal capacitance to minimize voltage unbalance and torque pulsations is performed. Moreover positive and negative components of voltages are revealed. A d-q-0 reference frame for dynamic performance analysis is used to investigate flux linkages and electromagnetic torque. The validity of the optimal capacitance is confirmed by experimental results, showing that the motor has the least voltage unbalance and the highest efficiency compared with other non-optimal capacitances. The experimental and simulation results are in good agreement.

**Streszczenie.** W artykule analizowano właściwości zmodyfikowanego trójfazowego silnika indukcyjnego. Na podstawie modelu matematycznego wyznaczono optymalną pojemność przy minimalnej liczbie zwojów oraz pulsację momentu. Określono też dodatnie i ujemne składowe napięcia. Zbadano też właściwości dynamiczne. Analiza właściwości zmodyfikowanego trójfazowego silnika indukcyjnego z optymalną pojemnością zasilanego napięciem jednofazowym

**Keywords:** Single-phase induction motors (SPIM), modified three-phase induction motor supplied with single-phase supply, voltage unbalance factor.

**Słowa kluczowe:** silnik indukcyjny, zmodyfikowany silnik trójfazowy zasilany napięciem jednofazowym

### Introduction

A Single-Phase Induction Motor (SPIM) plays an important role in low power household applications. It is employed in water pumps, washing machines, and air conditioners. However, when compared with a three-phase induction motor with the same power rating, the SPIM is more expensive, larger size, and heavier. Where a three-phase supply is unavailable, a three-phase induction motor can be modified to operate with a single-phase power supply by connecting a capacitor across one phase [1]. For this modified scheme, the motor stator winding voltages and currents are inevitably unbalanced thus resulting in decreased efficiency and torque pulsations. A degree of the voltage unbalance nevertheless can be minimized by selecting an appropriate capacitor value. With the optimal capacitance, the modified three-phase motor could operate as the same performance level as a SPIM. A mathematical model based on the approximation of state variables to calculate capacitors for the successful startup of a three-phase asynchronous motor fed by single-phase power supply has been presented [7]. However, this method is complicated and the electromagnetic torque has not been investigated.

Although balancing a three-phase induction motor supplied from a single-phase source with two SVCs has been proposed, only the simulation results have been given [8]. The disadvantage of a novel high-efficiency parallel-winding connection for a three-phase induction motor fed by a single-phase power supply using 2 dimensions finite element is the redundancy of a capacitor [9]. Although efficiency, torque against speed and power factor have been reported, the instantaneous electromagnetic torque was not given. An active-phase converter for the operation of three-phase induction motors on single-phase grid is complicated for control [10]. The thermal effect of voltage imbalance on stator windings can be found in [11]. Quantitative assessment such as torque, current, losses, efficiency and power factor of three-phase supply voltage unbalance effects on induction motors have been proposed [12]. The voltage unbalance factor (VUF) is used for this assessment. However, VUF for a three-phase standard induction motor supplied with a single-phase source has been rarely found. Besides, the effects of unbalanced voltages on the energy performance of three-phase

induction motors have been investigated [13]. Effects of voltage unbalance on torque and efficiency of a three-phase induction motor has also presented [15]. Although the instantaneous electromagnetic torque can be found in [16], the model seems to be complex. Only simulation results were given for comparison of induction motor on balanced and unbalanced voltages and capacitor phase splitter [17]. Effects of voltage unbalance and harmonic distortion on the torque and efficiency of a three phase induction motor have been given [18] [19]. However, there are a few publications for investigating performance particularly instantaneous electromagnetic torque under voltage unbalance of a three-phase induction motor supplied with a single-phase source. A three-phase induction supplied from a single-phase grid can operate as a generator [20][21].

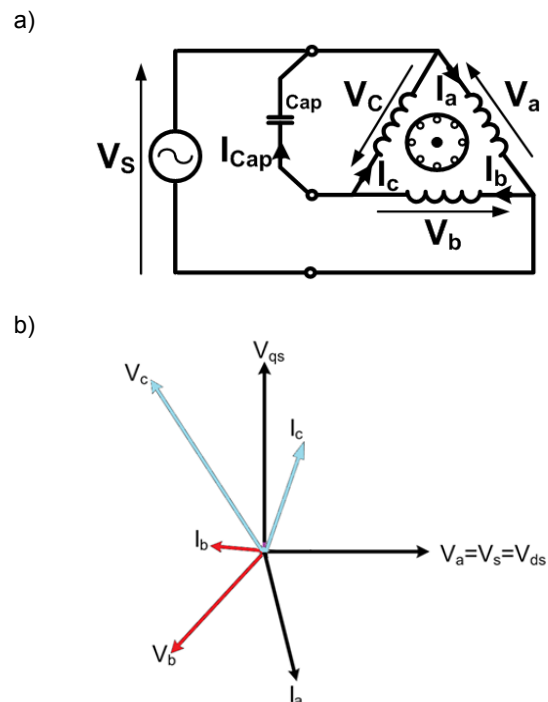


Fig.1. Modified Three-Phase Induction Motor (a) Modified three-phase induction motor for single-phase supply, (b) Phasor diagram for voltages and currents.

In this paper, the proposed simulation model using MATLAB/Simulink has been modified from [14]. According to the mentioned shortcomings, this paper proposes the originality of a capacitor selection based on symmetrical components solved from an unbalanced voltage problem, finding positive and negative components of voltages, comparison of VUF between calculation and experiment and use of d-q quantities in calculation of electromagnetic torque.

### Modified Three-Phase Induction Motor Description and analysis

The modified three-phase motor shown in Fig. 1(a) is a three-phase induction motor with a capacitor connected across one of its phases and energized by a single-phase AC supply. In the figure, the capital voltages and currents represent a phasor quantity.

The three-phase stator windings are connected in a delta configuration. The external capacitor,  $C_{cap}$ , is connected across a phase C winding. The AC input voltage is supplied to a phase A winding. Under this circumstance, the motor phase voltages and currents are inevitably unbalanced. For example, the corresponding phasor diagram can be depicted as shown in Fig. 1(b).

From Fig. 1(b), the following phasor relationships can be written: Stationary d-q model can be used for dynamic analysis. The relation between the voltage in d-q-0 axes can be expressed [1] as

$$(1) \begin{bmatrix} v_{qs} \\ v_{ds} \\ v_{0s} \end{bmatrix} = \sqrt{\frac{2}{3}} \begin{bmatrix} \cos \theta & \cos(\theta - 2\pi/3) & \cos(\theta + 2\pi/3) \\ -\sin \theta & -\sin(\theta - 12\pi/3) & -\sin(\theta + 2\pi/3) \\ \frac{1}{\sqrt{2}} & \frac{1}{\sqrt{2}} & \frac{1}{\sqrt{2}} \end{bmatrix} \times \begin{bmatrix} v_a \\ v_b \\ v_c \end{bmatrix}$$

In this equation,  $\theta = \omega_s \phi$ . The stator currents in d-q-0 axes can be given by

$$(2) \begin{bmatrix} i_{qs} \\ i_{ds} \\ i_{0s} \end{bmatrix} = \sqrt{\frac{2}{3}} \begin{bmatrix} \cos \theta & \cos(\theta - 2\pi/3) & \cos(\theta + 2\pi/3) \\ -\sin \theta & -\sin(\theta - 12\pi/3) & -\sin(\theta + 2\pi/3) \\ \frac{1}{\sqrt{2}} & \frac{1}{\sqrt{2}} & \frac{1}{\sqrt{2}} \end{bmatrix} \times \begin{bmatrix} i_a \\ i_b \\ i_c \end{bmatrix}$$

From the circuit in Fig. 1(a), the relation between voltages and currents can be obtained as follows.

$$(3) \left. \begin{aligned} v_s &= v_a \\ v_{cap} &= -v_c \\ p v_{cap} &= \frac{i_{cap}}{C} \\ i_{cap} &= i_c - i_b \\ i_s &= i_a - i_b \end{aligned} \right\}$$

Substituting (1) into (3) yields

$$(4) v_{ds} = v_a$$

$$(5) p v_{cap} = \frac{\sqrt{3}}{C} i_{qs}$$

$$(6) v_{qs} = \frac{1}{\sqrt{3}} v_{ds} - \frac{2}{\sqrt{3}} v_{cap}$$

$$(7) i_s = \frac{3}{2} i_{ds} + \frac{\sqrt{3}}{2} i_{qs}$$

The instantaneous electromagnetic torque [4] [22] is shown in terms of d-q-0 stator and rotor currents as

$$(8) \psi_{ds} = \int (v_{ds} - i_{ds} R_s) dt$$

$$(9) \psi_{qs} = \int (v_{qs} - i_{qs} R_s) dt$$

$$(10) \psi_s = \sqrt{\psi_{ds}^2 + \psi_{qs}^2}$$

$$(11) \psi_{md} = (\psi_{ds} - i_{ds} L_s)$$

$$(12) \psi_{mq} = (\psi_{qs} - i_{qs} L_s)$$

where  $\psi_{md}$  and  $\psi_{mq}$  are the magnetizing flux linkages and the mechanical equations of the machine can be given by

$$(13) T_e = \left( \frac{3}{2} \right) P (\psi_{md} i_{qs} - \psi_{mq} i_{ds})$$

$$(14) \omega_r = \int \frac{P}{2J} (T_e - T_L)$$

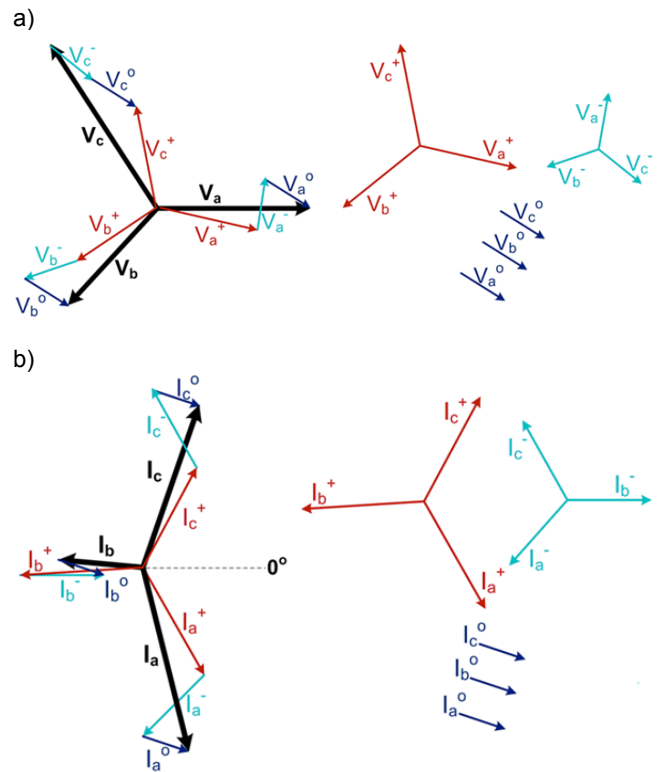


Fig.2. Symmetrical components to obtain three unbalanced components (a) Symmetrical components for three unbalanced components of voltages, (b) Symmetrical components for three unbalanced components of currents.

### Optimal capacitance calculation

The value of  $C_{cap}$  has a strong influence on motor operation. The capacitor that yields good motor starting performance often has poor performance at steady state whilst the capacitor giving poor starting performance provides good performance at steady state. Therefore, the capacitor selection practically involves a tradeoff between the motor starting and running performances. A three-phase induction motor normally operates with a balanced three-

phase sinusoidal supply. When the motor operates with a single-phase supply, it needs an external capacitor across one phase. As a result, imbalance of voltages and currents for each coil is inevitably present. The unbalanced voltages and currents can be depicted in Fig. 2. Hence instantaneous symmetrical component transformations can be used to solve such unbalanced systems. Each unbalanced phasor is the sum of positive sequence component, negative sequence component and zero sequence component as shown in Fig. 2(a) and Fig. 2(b)

The capacitor (Cap) in Fig. 1 is connected across the stator winding phase  $V_c$ . The relationships are as follows.

$$\begin{aligned} (15) \quad & v_a = v_s \\ (16) \quad & v_a + v_b + v_c = 0 \\ (17) \quad & v_c - j(i_b - i_c)X_{Cap} = 0 \\ (18) \quad & v_c = j(i_b - i_c)X_{Cap} \end{aligned}$$

The unbalanced motor voltages and currents can be written in terms of the symmetrical components as

$$(19) \quad \begin{bmatrix} v_a \\ v_b \\ v_c \end{bmatrix} = \begin{bmatrix} 1 & 1 & 1 \\ 1 & a^2 & a \\ 1 & a & a^2 \end{bmatrix} \begin{bmatrix} v^0 \\ v^+ \\ v^- \end{bmatrix}$$

$$(20) \quad \begin{bmatrix} i_a \\ i_b \\ i_c \end{bmatrix} = \begin{bmatrix} 1 & 1 & 1 \\ 1 & a^2 & a \\ 1 & a & a^2 \end{bmatrix} \begin{bmatrix} i^0 \\ i^+ \\ i^- \end{bmatrix}$$

where  $a$  is the transformation operator. The inverse transform of (21) is given by

$$\begin{aligned} a &= e^{j2\pi/3} = -\frac{1}{2} + j\frac{\sqrt{3}}{2} : a^2 = -\frac{1}{2} - j\frac{\sqrt{3}}{2} \\ &: (a^2 - a) = -j\sqrt{3} : (a - a^2) = j\sqrt{3} \end{aligned}$$

Substitution of (14) into the top row of (19) yields  $V^0 = 0$ . Since the zero-sequence voltage,  $V^0$ , is zero, the zero-sequence current,  $I^0$ , becomes zero as well. In other words, the zero-sequence components are absent from the delta connected motor in Fig. 1 and only the positive and negative sequence components remain. In this work, the value of Cap is selected such that the voltage unbalance on the motor windings is minimal. Note that by minimizing the voltage unbalance, the motor efficiency will be maximized. Mathematically, the optimal Cap can be calculated by (18).

$$(22) \quad av^+ + a^2v^- = jX_{cap}(a^2i^+ + ai^+ - ai^+ - a^2i^-)$$

$$(23) \quad U = \frac{v^-}{v^+} = \frac{[-a^2 - \sqrt{3}X_{cap}y^+]}{[a - \sqrt{3}X_{cap}y^-]}$$

$$(24) \quad U = \frac{\left[\frac{1}{2} + j\frac{\sqrt{3}}{2} - \sqrt{3}X_{cap}y^+\right]}{\left[-\frac{1}{2} + j\frac{\sqrt{3}}{2} - \sqrt{3}X_{cap}y^-\right]}$$

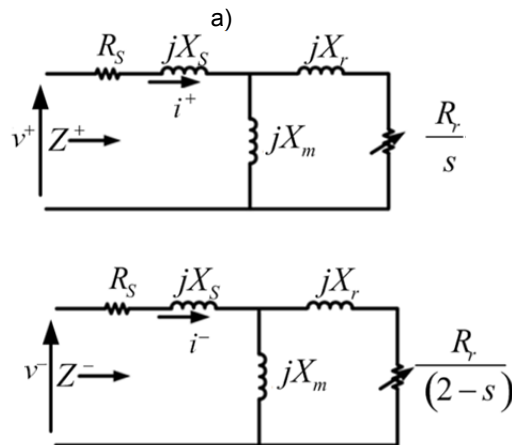


Fig.2. Induction motor equivalent circuits (a) positive sequence: S=Slip, (b) negative sequence: S=Slip.

Fig. 3 illustrates the induction motor equivalent circuits for the positive sequence in Fig. 3(a) and for negative sequence in Fig. 3(b) (22) indicates that the lesser the the negative sequence component, the closer the system becomes balance. If  $v^- = 0$  (i.e.  $U = 0$ ), the system will be perfectly balanced. (22) is rearranged as

$$(25) \quad U = \frac{\left[\frac{1}{2} + j\frac{\sqrt{3}}{2} - \sqrt{3}X_{cap}Y^+(\cos\phi_1 + j\sin\phi_1)\right]}{\left[-\frac{1}{2} + j\frac{\sqrt{3}}{2} - \sqrt{3}X_{cap}Y^-(\cos\phi_2 + j\sin\phi_2)\right]}$$

$$(26) \quad |U| = \frac{\left| \begin{aligned} &\left(\frac{1}{2} - \sqrt{3}X_{cap}Y^+\cos\phi_1\right)^2 \\ &+ \left(\frac{\sqrt{3}}{2} - \sqrt{3}X_{cap}Y^+\sin\phi_1\right)^2 \end{aligned} \right|^{\frac{1}{2}}}{\left| \begin{aligned} &\left(-\frac{1}{2} - \sqrt{3}X_{cap}Y^-\cos\phi_2\right)^2 \\ &+ \left(\frac{\sqrt{3}}{2} - \sqrt{3}X_{cap}Y^-\sin\phi_2\right)^2 \end{aligned} \right|^{\frac{1}{2}}}}$$

$$(27) \quad U = \frac{\left|1 + X_{cap}Y^+(-\sqrt{3}\cos\phi_1 - 3\sin\phi_1) + 3X_{cap}^2Y^{+2}\right|^{\frac{1}{2}}}{\left|1 + X_{cap}Y^- (\sqrt{3}\cos\phi_2 - 3\sin\phi_2) + 3X_{cap}^2Y^{-2}\right|^{\frac{1}{2}}}}$$

Let

$$D_1 = -\sqrt{3}\cos\phi_1 - 3\sin\phi_1$$

$$D_2 = \sqrt{3}\cos\phi_2 - 3\sin\phi_2$$

$$(28) \quad U = \frac{\left(1 + X_{cap}Y^+D_1 + 3X_{cap}^2Y^{+2}\right)^{\frac{1}{2}}}{\left(1 + X_{cap}Y^-D_2 + 3X_{cap}^2Y^{-2}\right)^{\frac{1}{2}}}$$

In this work, the value of  $C_{ap}$  is selected such that the voltage unbalance on the motor windings is minimal. Note that by minimizing the voltage unbalance, the motor efficiency will be maximized. Mathematically, the optimal  $C_{ap}$  can be calculated by taking the derivative of (28) concerning  $X_{Cap}$  and equating it to zero for determining minimum value of  $U$ , i.e.

$$(29) \quad \frac{dU}{dX_{Cap}} = 0$$

$$\frac{dU}{dx_{cap}} = \left( \frac{vdu}{dx_{cap}} - \frac{udv}{dx_{cap}} \right) \times \left( \frac{1}{v^2} \right)$$

where

$$u = \left( 1 + X_{Cap} Y^+ D_1 + 3 X_{Cap}^2 Y^{+2} \right)^{\frac{1}{2}}$$

$$v = \left( 1 + X_{Cap} Y^- D_2 + 3 X_{Cap}^2 Y^{-2} \right)^{\frac{1}{2}}$$

It can be rearranged as following equations.

$$(30) \quad 3Y^+ Y^- (Y^+ D_2 - Y^- D_1) X_{cap}^2 + 6(Y^{+2} - Y^{-2}) X_{cap}$$

$$+ (Y^+ D_1 - Y^- D_2) = 0$$

$$(31) \quad AX_{cap}^2 + BX_{cap} + C = 0$$

The coefficients in (31) are shown by

$$A = 3Y^+ Y^- (Y^+ D_2 - Y^- D_1)$$

$$B = 6(Y^{+2} - Y^{-2})$$

$$C = Y^+ D_1 - Y^- D_2$$

Table 1. Parameters of motor equivalent circuits

Parameter	Value
Stator resistance, $R_s$	1.5 $\Omega$
Stator leakage reactance, $X_s$	1.73 $\Omega$
Rotor resistance, $R_r$	1.0 $\Omega$
Rotor leakage reactance, $X_r$	1.73 $\Omega$
Magnetizing reactance, $X_m$	42.4 $\Omega$
Rated slip, $s$	0.033
Output	1.5 kW
Torque, $T_n$	10 Nm

A three-phase, 1.5kW, 4-pole, 50Hz, 1450rpm, 220V, 6A, delta-connected induction motor is used. As illustrated in Table1, the motor parameters are obtained by no load, blocked rotor, and DC resistance tests. These parameters, together with the rated slip=0.033, are used to solve (31) in MATLAB and the valid optimal capacitance is calculated to be approximately  $C_{ap} = 37.77\mu F$  but the close values of 35  $\mu F$  and 40  $\mu F$  are available by a manufacturer. Thus, the capacitor of 40  $\mu F$  was chosen

### Performance Evaluation

The main purpose of this experiment is to verify a the validity of the optimal capacitance (i.e.  $C_{ap} = 40\mu F$ ) and to measure the performance of the motor under direct online start and steady-state conditions when compared to other non-optimal capacitances. In the experiment, the modified motor was fed by a single-phase 220V, 50Hz AC mains supply at no-load condition. Its steady-state performance with three different values of  $C_{ap}$ , namely 40 $\mu F$ , 50 $\mu F$ , and

60 $\mu F$ , were measured. Note that for the lower capacitance than 40 $\mu F$ , the modified motor cannot a startup. The experimental results are presented in Figs. 4-6. By comparing the steady-state waveforms, it can be seen that the modified motor with the optimal capacitance,  $C_{ap} = 40\mu F$ , has the least unbalanced voltage and current of the motor windings as shown in Fig. 4(a)and(b).The unbalanced levels become more severed when  $C_{ap}$  is increased to 50 $\mu F$  and 60 $\mu F$  as shown in Fig. 5 and Fig. 6, respectively. These results confirm the validity of the optimal capacitance in minimizing the system unbalance.

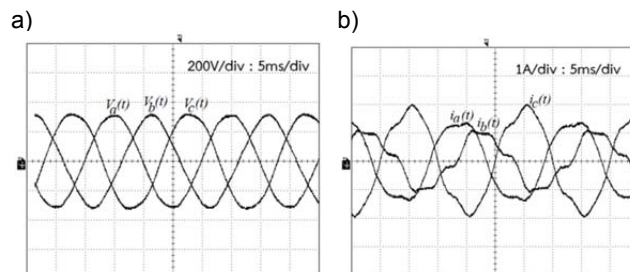


Fig. 4 Measured voltage: scale 200V/div, 5ms/div and current: scale 1A/div, 5ms/div of the modified three-phase motor with  $C_{ap} = 40\mu F$  (a) Phase voltage, (b) Phase current.

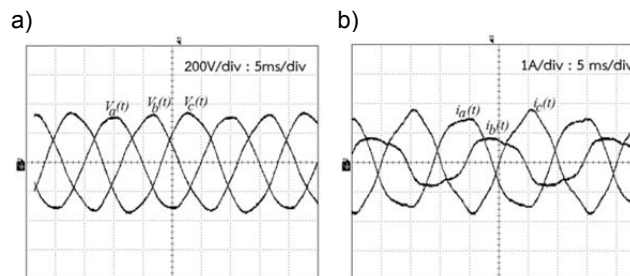


Fig. 5 Measured voltage: scale 200V/div, 5ms/div and current: scale 1A/div, 5ms/div of the modified three-phase motor with  $C_{ap} = 50\mu F$  (a) Phase voltage, (b) Phase current.

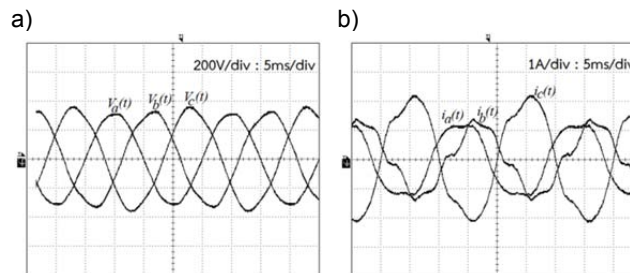
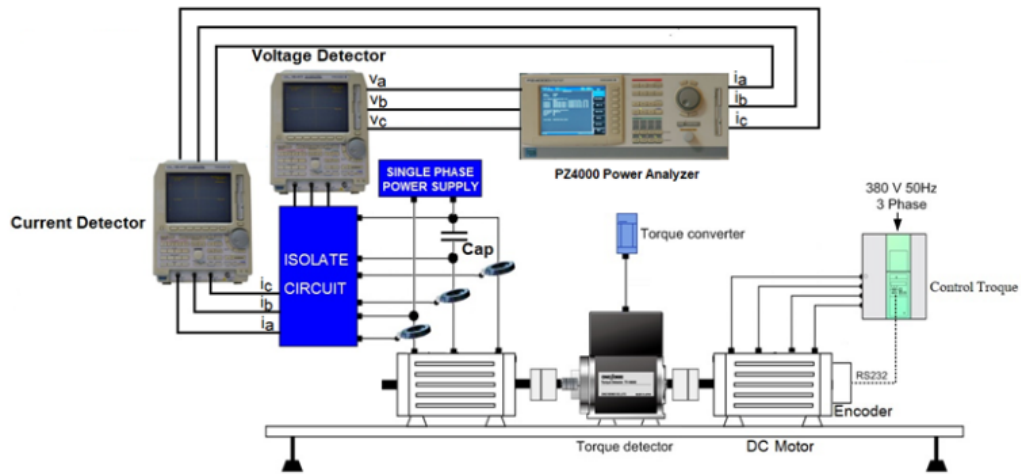


Fig. 6 Measured voltage: scale 200V/div, 5ms/div and current: scale 1A/div, 5ms/div of the modified three-phase motor with  $C_{ap} = 60\mu F$  (a) Phase voltage, (b) Phase current

Fig. 7 shows the experimental setup and photograph of the proposed system and equipment for performance evaluation. A DC motor is driven by SIMOREG DC Master 6RA70 Series Siemens is used for applied mechanical load. The mechanical torque and speed are measured by a torque transducer and a tachometer, respectively for measuring the mechanical output power. The input power is measured by using a power analyzer. Then the efficiency can be determined.

Fig. 8 illustrates the measured efficiency of the motor with the variation of the load torque. Obviously, the balanced three-phase supply gives the highest efficiency. The single-phase supply with various capacitances gives lower efficiency because of the imbalance of both voltage and current. The motor efficiency for 40  $\mu F$  is the highest when compared to that for 50  $\mu F$  and 60  $\mu F$  since both

phase voltage and current for 40  $\mu\text{F}$  have the lowest imbalance. Note that the rated load torque for the modified motor is one third of that for a standard three-phase induction motor as shown in Table 1. The relationships between  $U$  obtained from (28) and speed for capacitor a)



b)

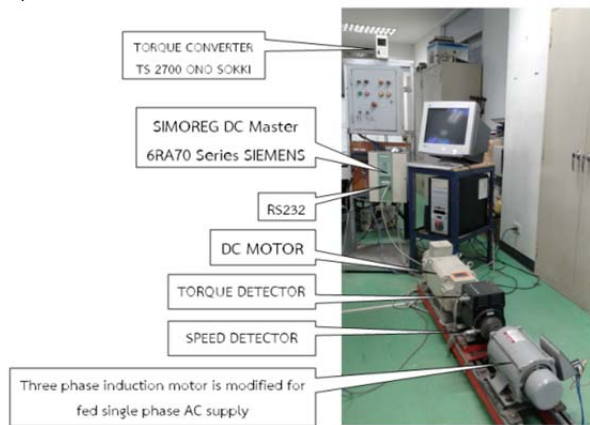


Fig. 7 The experimental set up of efficiency evaluation (a) The schematic diagram, (b) Photograph of the proposed system.

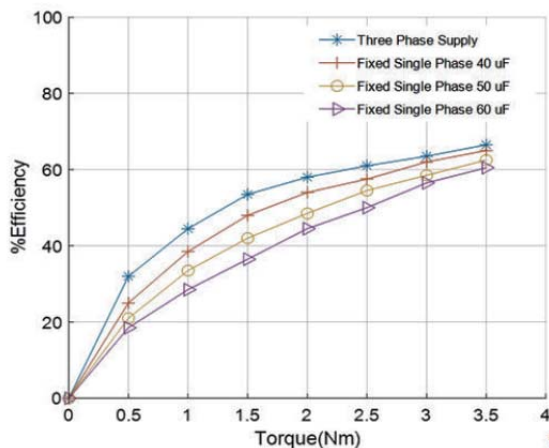


Fig. 8 Comparison of measured efficiency.

When the speed is increased (i.e. slip is decreased), the  $U$  values for various capacitances are decreased sharply and the differences of  $U$  for those capacitances are decreased too. Eventually, when the speeds reach their steady-state values, Cap = 40  $\mu\text{F}$  gives the lowest  $U$  value as shown in the zoom box in Fig. 9. This confirms that at low slip Cap = 40  $\mu\text{F}$  gives the lowest voltage imbalance resulting in the highest efficiency compared with other

values of 40 $\mu\text{F}$ , 50 $\mu\text{F}$  and 60 $\mu\text{F}$  ranging from the motor starting (i.e. high slip) to steady-state (i.e. low slip) are illustrated in Fig. 9. At high slip, the capacitor value of 60 $\mu\text{F}$  gives the lowest  $U$  value and the capacitor value of 50 $\mu\text{F}$  gives lower  $U$  value than the capacitor value of 40 $\mu\text{F}$ .

capacitances following Fig. 8. Fig. 10 shows the corresponding  $V^+$  and  $V^-$  versus slip with various capacitor values. When increasing the speed, the positive components for all capacitances are increased slightly whilst the negative components for all capacitances are decreased sharply in the same manner with the  $U$  values. The positive component and the negative component for 40  $\mu\text{F}$  are the highest for all values of slip. At high speed, the negative components for all capacitances are very close. This confirms that the optimal capacitance gives the lowest imbalance since it provides the highest positive component whereas the negative components for all capacitance are very close particularly for low slip (steady-state operating condition).

The % $U$  is defined by the International Electrotechnical IEC 60034-26:2006 Rotating electric machines–Part 26: Effect of unbalanced voltage on the performance of three-phase cage induction motors. The voltage unbalance factor (VUF) [6] which is a ratio of the negative-sequence voltage component to the positive-sequence voltage component can be given by (32). The higher positive component, the lower  $U$  value becomes particularly for low slip in accordance with Fig. 9 and Fig. 10. The comparative experimental results of % $U$ , experimental positive and negative sequence components of the motor operation under unbalanced voltages with various capacitances are illustrated in Table 2. Clearly the optimal capacitance gives the lowest of % $U$ .

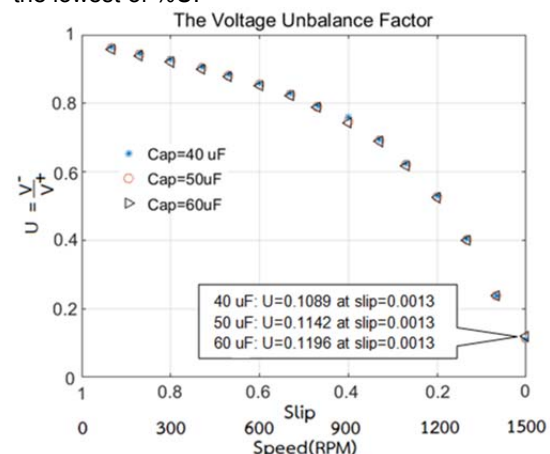


Fig. 9 Comparison of measured efficiency.

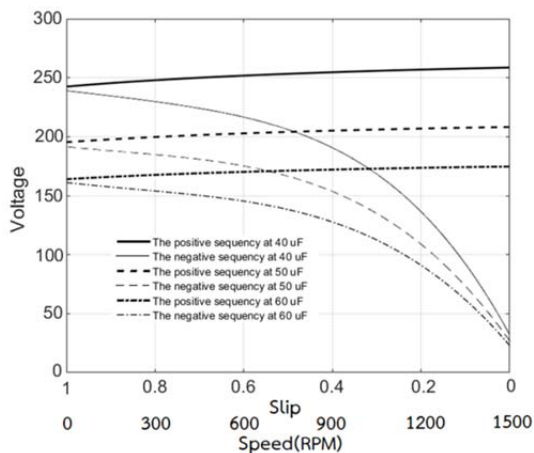


Fig. 10  $V^+$  and  $V^-$  versus slip with various capacitor values.

$$(32) \quad \%VUF = \%U = \frac{|V^-|}{|V^+|} \times 100\%$$

Table 1. The comparative experimental results of %U

Capacitor (Cap)	Experimental Results		
	%U	$V^-(RMS)$	$V^+(RMS)$
40 μF	4.2	226.63	9.5
50 μF	5.1	226.18	11.60
60 μF	5.6	226.13	12.16

A comparison of speed and current with a direct online start method between simulation and experiment for various capacitances is shown. The optimal capacitance of 40 μF offers the longest startup time whilst capacitance of 60 μF offers the lowest startup time. The higher capacitance, the lower startup time can be achieved. For all cases, the simulation and measured results are almost identical. These confirm the correctness of the obtained parameters and the used model.

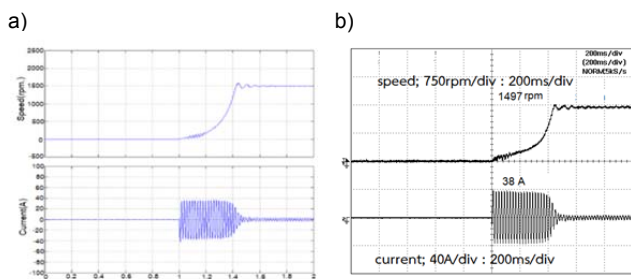


Fig. 11 Motor speed and starting current for  $C_{ap} = 40 \mu F$  (a) Calculated results, (b) Experimental results

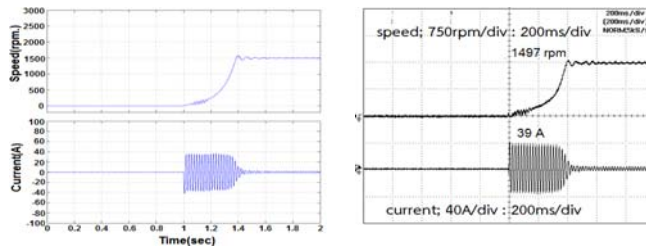


Fig. 12 Motor speed and starting current for  $C_{ap} = 50 \mu F$  (a) Calculated results, (b) Experimental results

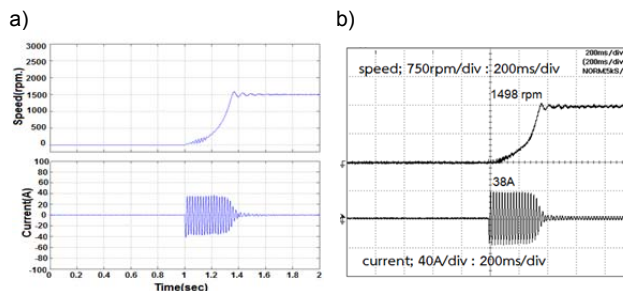


Fig. 13 Motor speed and starting current for  $C_{ap} = 60 \mu F$  (a) Calculated results, (b) Experimental results

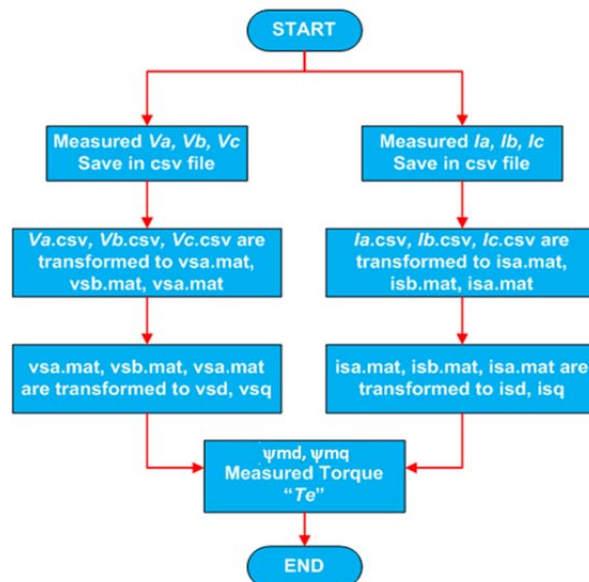


Fig. 14 Flow chart of finding torque.

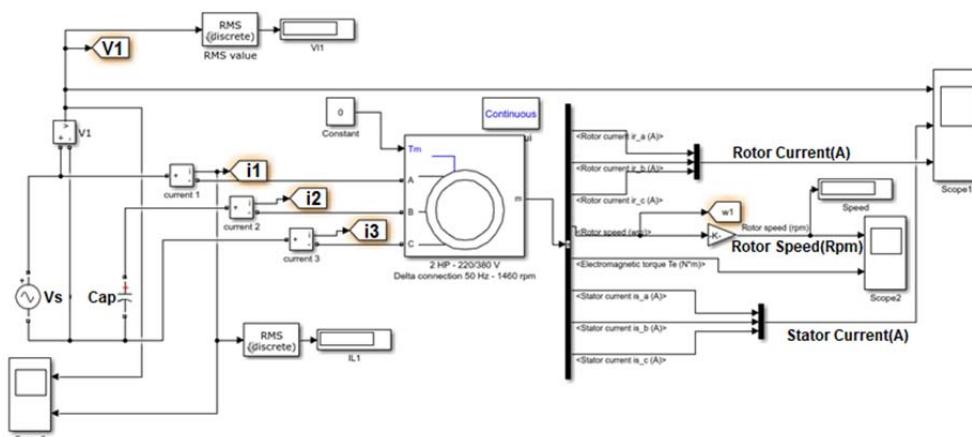


Fig. 15 The MATLAB/Simulink for calculating speeds

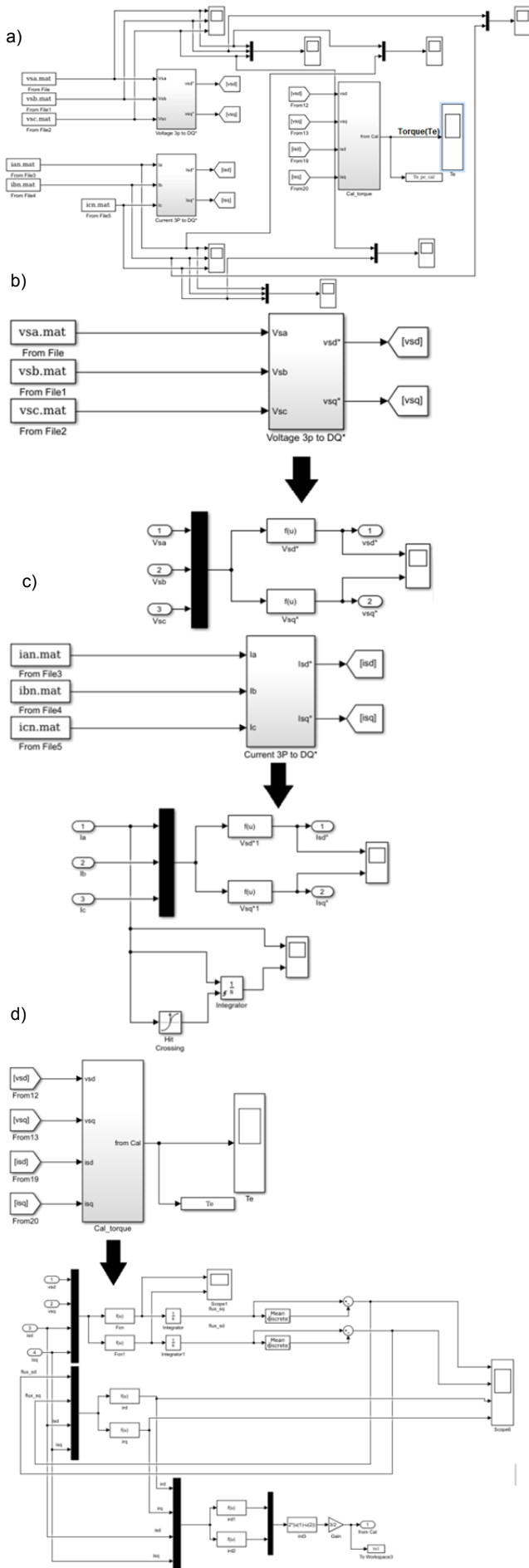


Fig. 16 The MATLAB/Simulink for finding torque (a) Overall block diagram for electromagnetic torque calculation, (b) Block diagram of d-q voltage calculation, (c) Block diagram of d-q current calculation, (d) Block diagram of electromagnetic torque equation  $T_e$

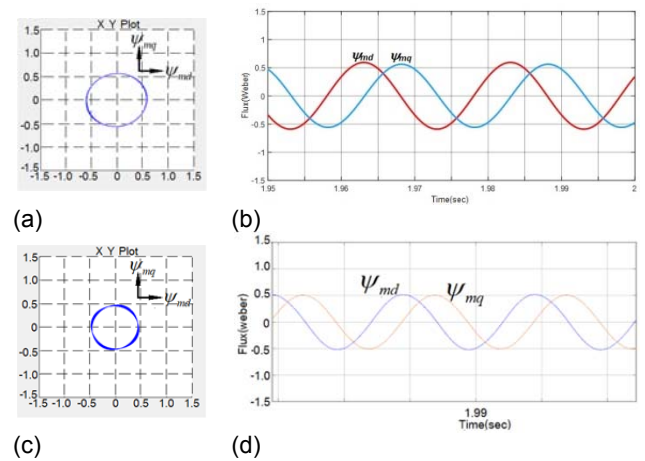


Fig. 17 Trajectories and waveforms of  $\psi_{md}$  and  $\psi_{mq}$  for  $C_{ap} = 40\mu F$ , (a) Calculated trajectory, (b) Calculated waveforms, (c) Measured trajectory, (d) Measured waveforms

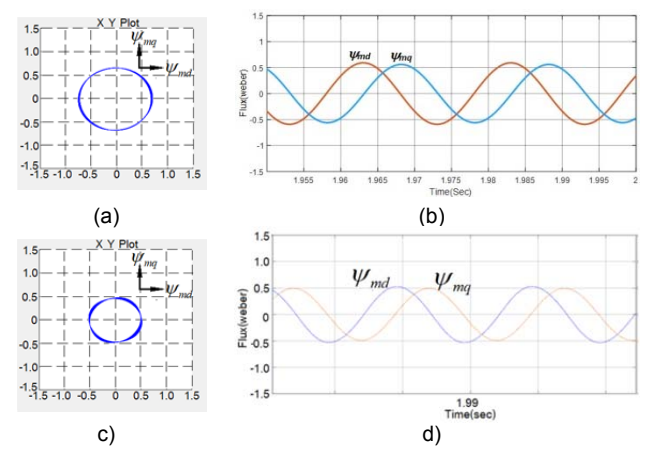


Fig. 18 Trajectories and waveforms of  $\psi_{md}$  and  $\psi_{mq}$  for  $C_{ap} = 40\mu F$ , (a) Calculated trajectory, (b) Calculated waveforms, (c) Measured trajectory, (d) Measured waveforms

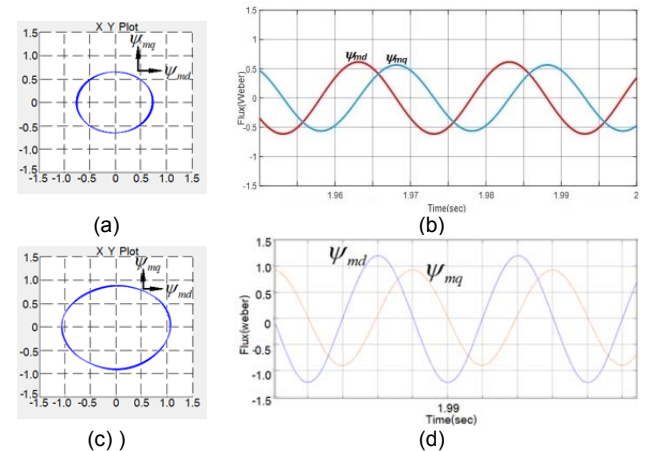


Fig. 19 Trajectories and waveforms of  $\psi_{md}$  and  $\psi_{mq}$  for  $C_{ap} = 40\mu F$ , (a) Calculated trajectory, (b) Calculated waveforms, (c) Measured trajectory, (d) Measured waveforms

By using (13), the instantaneous electromagnetic torque is calculated from the measured  $V_a, V_b, V_c$  and  $I_a, I_b, I_c$  which the data is recorded in an ASCII file. Then it is converted into a mat file for the calculation in following the flow chart as shown in Fig.14. Fig.15 and Fig.16 (a) (b),(c),and (d) show overall block diagrams, voltage and current block diagrams of calculation in d-q quantities, respectively using MATLAB/Simulink for calculating the electromagnetic torque. These block diagrams correspond to the flow chart.

Figs. 17-19 show a comparison of the magnetizing flux linkages  $\psi_{md}, \psi_{mq}$  between calculated results using(11) and (12) and experimental results for  $40\mu F, 50\mu F$  and  $60\mu F$ , respectively in terms of trajectory and waveform.  $Cap = 40\mu F$  which is the optimal capacitance gives the least imbalance since the amplitudes of  $\psi_{md}, \psi_{mq}$  are almost equal observed from waveforms especially for calculated results. The trajectory of flux linkages is almost circular. The calculated and measured results are in good agreement.  $Cap = 60\mu F$  which is non-optimal capacitance gives the highest difference in amplitudes of the magnetizing flux linkages, especially for measured results. The corresponding trajectory is distorted from a circular shape. It implies that the capacitance of  $60\mu F$  gives the highest imbalance of the voltages. Note that the higher imbalance level of flux linkages causes the higher ripple of the electromagnetic torque. Fig.20 (a)(b)(c)(d)(e)(f) shows a comparison of the calculated instantaneous electromagnetic torque with the experimental instantaneous electromagnetic torque between various capacitances. Apparently, the capacitance of  $40\mu F$  gives the lowest ripple torque at steady state.

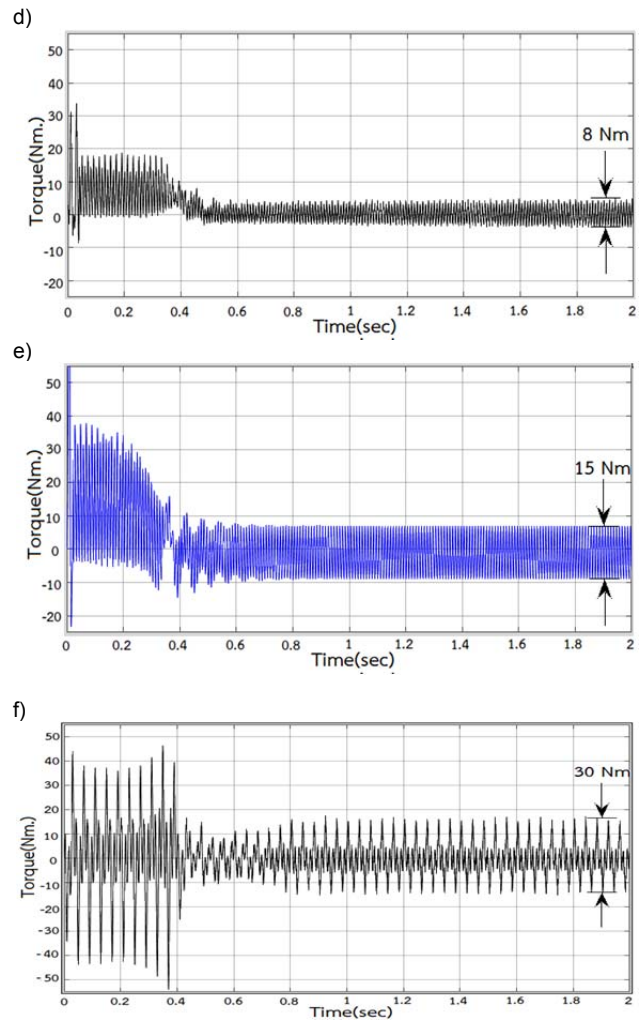
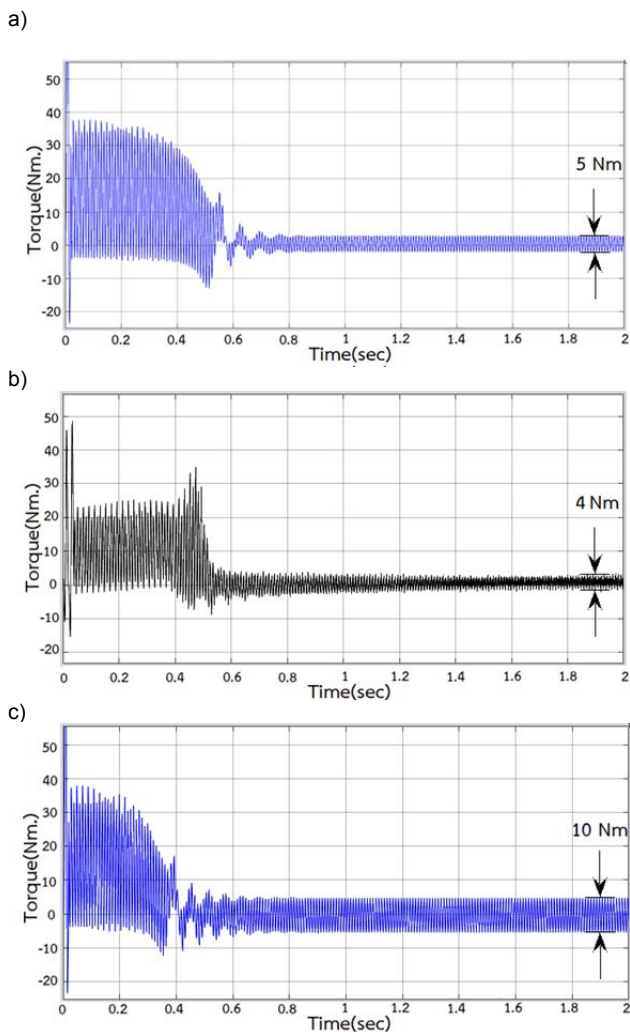


Fig. 20 The instantaneous electromagnetic torque, (a) Calculated results at  $40\mu F$ , (b) Experimental results at  $40\mu F$ , (c) Calculated results at  $50\mu F$ , (d) Experimental results at  $50\mu F$ , (e) Calculated results at  $60\mu F$ , (f) Experimental results at  $60\mu F$

## Conclusion

This paper has presented a performance analysis of a modified three-phase motor energized by a single-phase AC supply. The calculation method of the optimal capacitance to minimize the voltage unbalance has been fully described. The comparison of performances between various capacitances such as electromagnetic torque, flux linkages, efficiency, speed, positive and negative components of voltages and voltage unbalance factor has been given. When compared with other publications, this proposed technique reveals instantaneous electromagnetic torque, flux linkages and positive and negative voltage components. The voltage unbalance factor has been used for defining the degree of the imbalance. The selected optimal capacitance gives the lowest phase balancing and torque pulsations and the highest efficiency when compared with other non-optimal capacitances. In further work, the automatically adjustable capacitance for a wide range of operation using a static volt-amp-reactive (VAR) compensator will be implemented.

## Nomenclature:

$R_s, R_r$  - Stator and rotor resistances  
 $M, L_s, L_r$  - Mutual and stator and rotor self inductances  
 $i_{ds}, i_{qs}$  - Instantaneous d-q stator currents  
 $i_{dr}, i_{qr}$  - Instantaneous d-q rotor currents

$V_{ds}$ ,  $V_{qs}$  - Instantaneous d-q stator voltages  
 $V_{dr}$ ,  $V_{qr}$  - Instantaneous d-q rotor voltages  
 $V_{cap}$ ,  $C_{ap}$  - Instantaneous capacitor voltage and capacitance.  
 $\omega_r$ ,  $p$  - Rotor speed(rad/sec) and differential operator  $d/dt$   
 $T_e$ ,  $T_L$  - Developed torque and load torque  
 $J$  - Moment of inertia  
 $V_a, V_b, V_c$  - Instantaneous voltage  
 $i_a, i_b, i_c$  - Instantaneous current  
 $V_a^+, V_b^+, V_c^+$  - Positive sequence components instantaneous voltage  
 $V_a^-, V_b^-, V_c^-$  - Negative sequence components instantaneous voltage  
 $V_a^0, V_b^0, V_c^0$  - Zero sequence component phasor voltage  
 $I_a^+, I_b^+, I_c^+$  - Positive sequence components phasor current  
 $I_a^-, I_b^-, I_c^-$  - Negative sequence components phasor current  
 $I_a^0, I_b^0, I_c^0$  - Zero sequence component phasor current  
 $I_{ds}$ ,  $I_{qs}$ ,  $I_{os}$  - dq0 stator phasor currents  
 $I_{dr}$ ,  $I_{qr}$ ,  $I_{or}$  - dq0 rotor phasor currents  
 $V_{ds}$ ,  $V_{qs}$ ,  $V_{os}$  - dq0 stator phasor voltages  
 $Z^+$  - Positive sequence impedance  
 $Z^-$  - Negative sequence impedance  
 $V$  - Supply voltage  
 $Y^+$  - Magnitude of positive sequence admittance  
 $\phi_1$  - Angle of positive sequence admittance  
 $Y^-$  - Magnitude of negative sequence admittance  
 $\phi_2$  - Angle of negative sequence admittance  
 $\psi_{md}$ ,  $\psi_{mq}$  - Magnetizing flux linkages  
 $\psi_{ds}$ ,  $\psi_{qs}$  - Stator flux linkages  
 $P$  - Number of pole pairs  
 $\alpha$  - Transformation operator  
 $\omega$  - The angular velocity of signals to be transformed  
 $\varphi$  - The initial angle

#### Acknowledgement

The authors wish to thank Energy Policy and Planning office Ministry of Energy, Royal Thai Government for financial support. Also, this work was supported in part by the Thailand Research Fund under grant no. IRG5780006

#### Authors

**Chavaporn Bumroongphuck** was born in Bangkok, Thailand. He received M.Eng. degree in electrical engineering from King Mongkut's Institute of Technology Ladkrabang, Bangkok, Thailand, in 2006. He is currently pursuing his D. Eng. degree at King Mongkut's Institute of Technology Ladkrabang, Bangkok, Thailand Since 2012. His research interests include power electronics, electrical machines and electric drives

**Vijit Kinnares** (Member, IEEE) was born in Sakon Nakhon, Thailand. He received the B.Eng. and M.Eng. degree in electrical engineering from King Mongkut's Institute of Technology Ladkrabang, Bangkok, Thailand, and received the Ph.D. degree in electrical engineering from University of Nottingham, England. Currently, he is an Assoc. Professor at King Mongkut's Institute of Technology Ladkrabang. His research interests include renewable energy systems, power electronics and drives.

#### REFERENCES

- [1] P. C. Sen, Principle of electric machines and power electronics: John Wiley & Sons 3<sup>rd</sup> edition 2013.
- [2] Prado Wellington, Gonc, alves de Mendonca, a Roberlam and Martins Neto Luciano, "Comparative performance analysis of a standard three-phase induction motor and an asymmetric three-phase induction motor fed from a single-phase network" *ELSVIER*.Vol.125,pp.211-219,Aug.2015.
- [3] Veera Thanyaphirak, Vijit Kinnares and Anuntawat Kunakom, "Soft starting control scheme for three-phase induction motor fed by PWM AC chopper," *IMECS International Multi Conference*, pp.92-95,Oct.2014.
- [4] Veera Thanyaphirak, Vijit Kinnares and Anuntawat Kunakom, "Comparison of starting current characteristics for three-phase induction motor due to phase-control soft starter and asynchronous pwm ac chopper," *JEET*, Vol. 12, No. 3, pp. 1921-1931,May.2017.
- [5] Said A. Deraz and Haitham Z. Azazi, "Current limiting soft starter for three phase induction motor drive system using pwm ac chopper," *IET Power Electronics*, Vol. 10, pp.1289-1306, Sep. 2017.
- [6] A.I. Adekitan, Ayodeji Samson Ogunjuigbe, Raphael Ayodele and Isaac Adekunle Samuel, "The performance of a 3-Phase Induction Machine under Unbalance Voltage Regime." *Journal of Engineering Science and Technology Review*, Vol. 10, No. 5, pp.136-143, Nov. 2007.
- [7] Vasily Malyar, Orest Hamola and Volodymyr Maday, "Calculation of capacitors for starting up a three-phase asynchronous motor fed by single-phase power supply," *IEEE Computational Problems of Electrical Engineering*, Sep 2016.
- [8] Yaw-Juen Wang, Lambert Pierrat and Elena Helerea, "Balancing a Three-Phase Induction Motor Supplied from a Single-Phase Source with Two SVCs," *ACEMP on*, pp.268-274, May. 2017.
- [9] Yaw-Juen Wang, Lambert Pierrat and Elena Helerea, "Balancing a Three-Phase Induction Motor Supplied from a Single-Phase Source with Two SVCs," *ACEMP on*, pp.268-274,May.2017.
- [10] Anil K. Adapa and Vinod John, "Active-Phase Converter for Operation of Three-Phase Induction Motors on Single-Phase Grid," *IEEE Transactions on Industry Applications*, pp.5668-5675, Aug. 2017.
- [11] Jose L. Gonzalez-Cordoba, Roque A. Osornio- Rios, David Granados-Lieberman and Rene De J. Romero, "Correlation Model Between Voltage Unbalance and Mechanical Overload Based on Thermal Effect at the Induction Motor Stator," in *IEEE TRANSACTIONS ON ENERGY CONVERSATION*, Vol 32, No.4, pp.1602-1610,June.2017.
- [12] Larbi Refoufi and Hamid Bentarzi, "Quantitative assessment of three phase supply voltage unbalance effects on induction motors," *International Journal of System Assurance Engineering and Management*, Vol 8, No.1, pp. 393-460, Jan. 2017.
- [13] Joseph Vardi and Benjamin Avi-Itzhak, "Electric Energy Generation; Economics, Reliability and Rates," MIT, 1981, p.75-94
- [14] Hoang Le-Huy, "Modeling and simulation of electrical drives using MATLAB/Simulink and Power System Blockset," *IECON' Annual Conference of the IEEE Industrial Electronics Society*, Aug. 2002.
- [15] Ana Bárbara Fernandes Neves, Anésio de Leles Ferreira Filho and Marcus Vinícius Borges de Mendonça, "Effects of Voltage Unbalance on Torque and Efficiency of a Three-phase Induction Motor," *ICHQP*, pp. 679-683, June. 2014.
- [16] Jannati, Mohammad, Sutikno Tole, Idris, Nik Rumzi Nik; Aziz and Mohd Junaidi Abdul, "Modeling of Balance and Unbalance Three-Phase Induction Motor under Balanced and Unbalanced Supply Based on Winding Function Method," *IJECE*, Vol. 5, pp.644-655, Aug. 2015.
- [17] M.G Hudedmani, A. Banu, I. Hiremath, P. Meghna and S. Yaligar, "Simulation and comparison of Induction Motor on Balance/unbalance supply and Capacitor phase splitter," *International Journal of Advanced Reserch Foundation*, pp.62-70.
- [18] Ana Bárbara Fernandes Neves, Marcus Vinícius Borges de Mendonça and Anésio de Leles Ferreira Filho, "Effects of Voltage unbalance and Harmonic Distortion on the Torque and Efficiency of a three Phase Induction Motor," *IEEE Harmonics and Quality of Power*, pp. 943-948, Otc. 2016.
- [19] M. Memon, A.K. Junejo and M. Siyal, "Performance Analysis of Induction Motor Operating at Unbalance Under and Overvoltage supply-A comparative approach," *IEEE Harmonics and Quality of Power*, Vol. 1, No. 1, pp.32-37, Apr. 2017.
- [20] S. Yukhalang, B. Sawetsaklanond and V. Kinnares, "Performance Evaluation of a Single-Phase Grid Connected Induction Generator," *ICEMS*, pp.3148-3153, Oct. 2014.
- [21] Maher Al-Badri, Pragasen Pillay and Pierre Angers, "A Novel In Situ Efficiency Estimation Algorithm for Three-Phase Induction Motors Operating with Distorted Unbalanced Voltages," *IEEE Energy Conversion Congress and Exposition*, Feb. 2016.
- [22] Gonçalves de Mendonça Roberlam and Martins Neto Luciano, "Comparative performance analysis of a standard three-phase induction motor fed from a single-phase network," *ELSVIER. Electric Power systems Research*, Vol. 125, pp.211-219, Aug. 2015.